HHS Public Access

Author manuscript

ACS Photonics. Author manuscript; available in PMC 2022 April 19.

Published in final edited form as:

ACS Photonics. 2021 June 16; 8(6): 1673–1682. doi:10.1021/acsphotonics.1c00045.

Enhancing Single-Molecule Fluorescence Spectroscopy with Simple and Robust Hybrid Nanoapertures

Abhay Kotnala,

Walker Department of Mechanical Engineering and Texas Material Institute, The University of Texas at Austin, Austin, Texas 78712, United States

Hongru Ding,

Walker Department of Mechanical Engineering, The University of Texas at Austin, Austin, Texas 78712, United States;

Yuebing Zheng

Walker Department of Mechanical Engineering and Texas Material Institute, The University of Texas at Austin, Austin, Texas 78712, United States;

Abstract

Plasmonic nanoapertures have found exciting applications in optical sensing, spectroscopy, imaging, and nanomanipulation. The subdiffraction optical field localization, reduced detection volume (~attoliters), and background-free operation make them particularly attractive for single-particle and single-molecule studies. However, in contrast to the high field enhancements by traditional “nanoantenna”-based structures, small field enhancement in conventional nanoapertures results in weak light–matter interactions and thus small enhancement of spectroscopic signals (such as fluorescence and Raman signals) of the analytes interacting with the nanoapertures. In this work, we propose a hybrid nanoaperture design termed “gold-nanoislands-embedded nanoaperture” (AuNIs-e-NA), which provides multiple electromagnetic “hotspots” within the nanoaperture to achieve field enhancements of up to 4000. The AuNIs-e-NA was able to improve the fluorescence signals by more than 2 orders of magnitude with respect to a conventional nanoaperture. With simple design and easy fabrication, along with strong signal enhancements and operability over variable light wavelengths and polarizations, the AuNIs-e-NA will serve as a robust platform for surface-enhanced optical sensing, imaging, and spectroscopy.

Graphical Abstract

Corresponding Author: **Yuebing Zheng** – Walker Department of Mechanical Engineering and Texas Material Institute, The University of Texas at Austin, Austin, Texas 78712, United States; zheng@austin.utexas.edu.

Author Contributions

The manuscript was written through contributions of all authors. All authors have given approval to the final version of the manuscript.

Supporting Information

The Supporting Information is available free of charge at https://pubs.acs.org/doi/10.1021/acsphotonics.1c00045.

Supplementary figures and Supplementary Notes 1–5 (PDF)

Complete contact information is available at: https://pubs.acs.org/10.1021/acsphotonics.1c00045

The authors declare no competing financial interest.

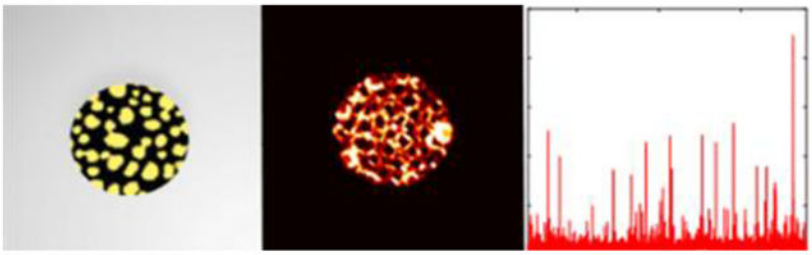

Keywords

nanoholes; fluorescence enhancement; fluorescence spectroscopy; nanoantenna; gold nanoislands

Plasmonic nanoapertures have shown great potential in optical sensing,[1–5] spectroscopy,[6–9] imaging,[10,11] nano-fabrication,[12,13] trapping,[14–16] and nonlinear photonics.[17] With their capacities of localizing electromagnetic field to subdiffraction regions, reducing detection volume to attoliters, and enabling background-free optical detection, nanoapertures are particularly attractive for scientific studies at the single-molecule level.[18–20] For example, their use in performing fluorescence correlation spectroscopy has enabled single-analyte characterization at high micromolar concentrations.[21,22] As optical nanotweezing elements, the nano-apertures have been used for sensing or analyzing various nanoparticles such as quantum dots,[23,24] proteins,[25,26] and DNA[27,28] with single-molecule resolution. The nanoapertures have even found uses in commercial applications such as gene sequencing[29] and near-field scanning optical microscopy.[30]

Still, the use of nanoapertures remains limited because of their small field enhancement. For example, a metal nanosphere when excited at surface plasmon resonance provides a strong near-field enhancement, which is more than five times larger than that provided by its “equivalent”, i.e., a circular nanoaperture in a metal film.[31–33] It should be noted that we do not classify nanoapertures as “nanoantennas”, which refer to conventional “nanoantenna” structures (e.g., plasmonic nano-pillars and nanoparticle dimers),[34,35] simply because of their poor antenna characteristics of coupling far-field light into localized regions or vice versa. The small field enhancement leads to weak light–matter interactions within the nano-aperture, limiting the enhancement of spectroscopic signals (e.g., fluorescence and Raman) from molecules interacting with the nanoaperture.[8,21,36–43] In comparison, conventional “nanoantenna” structures have shown stronger enhancement in the spectroscopic signals from the nearby molecules.[44–48] Such “nanoantenna” structures range from a single nanosphere[31,49–51] or nanorod[52,53] to the more complex engineered nanostructures such as dimers,[49,54–56] bowtie,[57,58] and Yagi-Uda.[59] However, for many of the “nanoantenna” structures, the strong field enhancements rely on small nanogaps with dimensions of <10 nm in the structures, which often require expensive and low-throughput nanofabrication tools such as electron-beam lithography. In addition, the “nanoantenna” structures for enhanced molecular spectroscopy are prone to background signal from molecules diffusing within the diffraction-limited excitation source and their uses for the single-molecule studies often require molecular concentrations lower than picomolar. Nanoapertures provide a promising alternative for enhanced molecular spectroscopy due to their low detection volumes and

background-free operation. To further enhance the optical signals from molecules at the nanoapertures, several techniques have been proposed to increase the local-field intensity at the nanoapertures by incorporating additional light management structures such as corrugations,[60] photonics crystals,[61] and “antenna-in-box”.[62] However, these additional structures involve strict design principles, specific nanoaperture geometries, and complex fabrication.

In this work, we propose a simple hybrid nanoaperture design termed “gold-nanoislands-embedded nanoaperture” (AuNIs-e-NA), which creates multiple electromagnetic “hotspots” to strongly enhance the local-field intensities within the nanoaperture and to boost the performance of the nano-aperture-enhanced fluorescence spectroscopy (Figure 1a). The strong field enhancement arises from the gap plasmon resonances excited at the networks of randomly distributed gold nanoparticles constituting the AuNIs within the nano-aperture (Figure 1b).[63,64] We show that the presence of multiple high-intensity “hotspots” within the nanoaperture can significantly enhance fluorescence signals from single molecules interacting with the nanoaperture. In addition, the scattering from the AuNIs also enhances the light coupling out from the nanoaperture, serving as a nanoantenna. In addition to the strong field enhancement and enhanced light coupling, the AuNIs-e-NA provides several more benefits to enhancing fluorescence spectroscopy. For example, in the AuNIs-e-NA, multiple small nanogaps that sustain the “hotspots” are created in a much simpler way as compared to the initial demonstrations of the “antenna-in-box” designs, which required focused-ion beam (FIB) or electron beam lithography (EBL) to achieve the nanogaps.[62] Recently, designer nanoantennas fabricated by simpler and highly scalable methods with superior control of nanogaps similar to that illustrated in our work have also been reported.[65–68] It should be noted that we use the term “nanogaps” to define the smallest interparticle distances between any two adjacent Au nanoparticles constituting the AuNIs (see Supporting Information, Figure S1). The term “nanogap” is generally attributed to the spacing between the two elements of a dimer nanoantenna. It might not be appropriate in a stricter sense when used for AuNIs that consist of closely packed multiple nanoparticles. However, one can interpret the AuNIs as a network of randomly arranged dimer nanoantennas coupled to each other, and therefore we define the smallest distances between any two adjacent nanoparticles (i.e., interparticle distances) as “nanogaps” in this work. The multiple “hotspots” instead of a single one can provide better signal enhancements, particularly when dealing with analytes larger than the nanogap sizes, due to the larger overlap of the analytes with the high-intensity electromagnetic regions.

Furthermore, due to the different sizes, shapes, gap dimensions, and orientations of the gold nanoparticles in a AuNIs-e-NA, it is responsive to and thus allows the spectroscopic operation over a wide range of wavelengths and polarizations of working light, which contrasts with “antenna-in-box” geometry, which requires a specific wavelength and polarization. Finally, the AuNIs-e-NA can be implemented with nanoapertures of arbitrary shapes and sizes, as the nanoapertures do not strongly influence the overall characteristics of the nanoislands and their “hotspots”. In contrast, for other hybrid structures where nanoapertures can significantly influence nanoantenna properties or vice versa, one must rationally design the nanoapertures and the nanoantennas and sometimes make a trade-off between these two subunits, limiting their optimum performance. With its simple design,

easy fabrication, and applicability to various working light ranges, in combination with the strong field enhancements comparable to “nanoantenna”-based structures, AuNIs-e-NAs present an advancement over conventional nanoapertures for enhanced applications in optical spectroscopy, sensing, imaging, and trapping of single nanoparticles and molecules.

As shown in Figure 1a, the AuNIs-e-NA combines the advantages of both the “nanoaperture” and “nanoantenna” geometries in a single structure for enhanced fluorescence spectroscopy of single-molecular analytes. The nanoaperture in a silver (Ag) thin film can confine light below the diffraction-limited confocal volume and hence provide detection volume as low as zeptoliters. At the same time, it becomes feasible to reduce or completely block the background signal by avoiding the excitation of molecules outside the nanoaperture volume, enabling single-molecule measurement with high signal-to-noise ratio (SNR). Furthermore, the AuNIs within the nanoaperture, which consist of closely packed gold nanoparticles with sub-40 nm gaps, serve as “nanoantenna” structures and feature multiple “hotspots” with strong local-field intensities. The AuNIs can further reduce the background signal and improve the SNR by confining excitation light to the bottom surface (i.e., AuNIs at the Ag–glass interface in Figure 1a) of the nanoaperture and preventing the direct excitation of molecules diffusing within the nanoaperture volume (see Supporting Information, Figure S2).

We fabricated the AuNIs-e-NAs using colloidal lithography[69–71] (see Methods section: Sample Fabrication). Briefly, AuNIs were first fabricated on a glass coverslip, followed by the formation of nanoapertures on the AuNIs substrate using polystyrene particles as masks. In Figure 1a, the AuNIs-e-NA was circular with a diameter of 200 nm and made in a Ag film with a thickness of 100 nm. The AuNIs within the nanoaperture consist of high-density randomly distributed Au nanoparticles with sizes of 20–60 nm and interparticle distances of 10–40 nm (see Supplementary Note 1). Figure 1b shows the scanning electron microscope (SEM) image of a representative AuNIs-e-NA. Thousands of AuNIs-e-NAs can be fabricated on a single coverslip using colloidal lithography, making the fabrication process simple, scalable, and cost-effective. For comparisons, a section of the coverslip was masked during the AuNI fabrication, which resulted in the formation of conventional nanoapertures in the metal film as shown in Figure 1c. The fabrication of both the AuNIs-e-NA and conventional nanoaperture on the same substrate minimized the structural variations between the two kinds of nanoapertures and enabled optical measurements under identical experimental conditions for accurate performance comparisons. From the optical transmission spectra, we can see that a strong absorption in the 500–700 nm range occurred for the AuNIs-e-NA (Figure 1d), which indicated the presence of AuNIs within the nanoaperture.[72] The simulated far-field transmission spectrum of the AuNIs-e-NA showed a similar optical absorption behavior (see Supporting Information, Figure S3).

To quantify the field enhancement provided by the AuNIs-e-NA in comparison to a conventional nanoaperture, we calculated the normalized electric-field intensities within these two nanoapertures. Figure 2a shows the variations in the total electric-field intensities simulated for a AuNIs-e-NA and a conventional nanoaperture as a function of excitation light wavelength. The AuNIs-e-NA exhibits an increased field intensity within the nanoaperture for the entire visible and near-infrared regime of the spectrum with a

maximum at ~900 nm. Figure 2b and c show the distributions of the normalized electric-field intensity within the AuNIs-e-NA and conventional nanoaperture, respectively, when excited by a circularly polarized light with a wavelength of 785 nm (see Methods section: Numerical Simulations). The AuNIs-e-NA features many high-intensity regions within the nanoaperture with a maximum field enhancement of >1000 (Figure 2d). This is in direct contrast to the almost uniform field enhancement of ~8 at the conventional nanoaperture (Figure 2b and d). The field enhancement of the AuNIs-e-NA arises from the excitation of gap plasmon resonances at the AuNIs. By tuning the size, shape, spatial distribution, and material composition of the nanoislands within the nanoaperture, we can easily tune the magnitude of the field enhancement, the number of "hotspots", and the working wavelength of the AuNIs-e-NA for targeted applications. This can be achieved by controlling the Au layer thickness and the annealing process (i.e., annealing temperature and time) during the AuNI fabrication process.[73] For example, by increasing the Au layer thickness (set to ~4.5 nm in our case), one can increase the nanoantenna sizes and shift the plasmon resonance peak to longer wavelengths. Similarly, by increasing the annealing temperatures and time, one can increase the gap sizes with the morphology of the nanoparticles becoming more spherical.[74] Repeated dewetting of thin gold films has also been used to control the nanoparticle gaps to very small sizes.[63] Therefore, with proper control of the AuNIs' fabrication parameters, one can moderately tune the size, shape, and gap of the nanoantennas in the AuNIs-e-NA. Still, our fabrication method lacks the precision provided by advanced nanofabrication methods such as EBL and FIB.

It should be noted that we have used Ag films to fabricate our AuNIs-e-NA primarily due to the availability and cost-effectiveness of Ag to produce thick metal films (~100 nm) that can eliminate the background signal by blocking the residual laser beam. We have shown that a 100 nm Ag film minimizes the background signal and maximizes the local-field intensity within the AuNIs-e-NA (see Supplementary Note 2). Alternative metals such as gold and aluminum can also be used to fabricate the AuNIs-e-NA, as they also show strong local-field enhancement and low background signal needed for enhanced single-molecule fluorescence spectroscopy at the visible and near-infrared (NIR) wavelengths (see Supplementary Note 3). A AuNIs-e-NA made in Au films would be more appropriate for biological analytes due to the better stability and biocompatibility of Au compared to Ag, which can be toxic and degrade over time.

Due to the random distribution and orientation of the nanoparticles within the AuNIs-e-NA, and the dependence of gap plasmon modes on the polarization of excitation light, different nanogap regions in the network of nanoparticles within the AuNIs-e-NA are excited at different light polarizations to enable the equivalent local-field enhancements (see Supporting Information, Figure S9a and b). This polarization "independence" allows operation of a AuNIs-e-NA with an arbitrary polarized or even unpolarized excitation light. A further study reveals that a circularly polarized laser beam excites the maximum number of gap regions and thus "hotspots" at the AuNIs within the nanoapertures (see Supporting Information, Figure S9c). The excitation of the greater number of "hotspots" within a AuNIs-e-NA with a circularly polarized light is also evident from the enhanced Raman spectroscopy of analyte molecules, where the stronger Raman signals were obtained

from the AuNIs-e-NA when excited using circularly polarized light compared to linearly polarized light (see Supporting Information, Figure S10).

Due to the variable nanoparticle sizes, shapes, orientation, and gaps in the AuNIs, the AuNIs-e-NA can exhibit strong field enhancements over a wide range of excitation light wavelengths as shown in Figure 2a. We further investigated the local-field intensities of the AuNIs-e-NA upon excitation by laser beams at two different wavelengths (i.e., 532 and 660 nm) in the visible light regime, which are most commonly used in performing fluorescence spectroscopy (see Supporting Information, Figures S11 and S12). The AuNIs-e-NA exhibits higher local-field intensities than the conventional nano-aperture for both excitation laser beams. The 785 nm laser beam (Figure 2c and d) leads to a larger magnitude of local-field enhancement and number of “hotspots” in the AuNIs-e-NA than the 532 nm (Figure S11b and c) and 660 nm (Figure S12b and c) laser beams due to the gap plasmon resonance peaks occurring in the NIR regime (Figure 2a). In comparison to many previous approaches proposed for improving the field enhancement in nanoapertures,[60,62,75] the AuNIs-e-NA has multiple advantages, including easy and scalable fabrication with colloidal lithography and applicability to a wide range of working laser beams of variable wavelengths and polarizations. With its strong field enhancement, the AuNIs-e-NA is expected to boost the performances of various surface-enhanced optical spectroscopies.

Herein, we chose single-molecule fluorescence spectroscopy to demonstrate the enhanced spectroscopic performance of the AuNIs-e-NAs over conventional nanoapertures. Fluorophores with intrinsically low quantum yield were chosen for measuring the maximum fluorescence signal improvement by AuNIs-e-NAs with reference to conventional nanoapertures. Such fluorophores would provide larger fluorescence enhancement factors due to the relatively larger contribution of the field enhancement to the overall fluorescence signal. We chose a near-infrared dye, indocyanine green (ICG) (excitation/emission wavelengths: 789/817 nm; quantum yield: 5%),[76,77] as the analyte due to the overlap of its absorption and emission spectra with the wavelengths corresponding to the strong field enhancements in the AuNIs-e-NA as shown in Figure 2a. ICG molecules were excited using a 785 nm laser beam. To measure the fluorescence signal from a single fluorophore molecule, the nanoapertures were covered by a solution containing the fluorescent dye with a concentration of 100 nM. At this concentration, there is ~0.1 fluorophore molecule within the nanoaperture volume (3 attoliters), enabling single-molecule measurements. The fluorophore solution was prepared in 1:1 water–glycerol solvent to reduce the diffusion time of the fluorophores so that the fluorescence signal could be directly used to measure the intensity bursts arising from individual fluorophore molecules (see Methods section: Chemicals for Fluorescence and Raman Spectroscopies). The fluorescence signal from individual molecules was measured as the fluorophores constantly diffused in and out of the nano-aperture due to the Brownian motion. The fluorescence signal from the nanoapertures was collected in the back-reflection mode (see Methods section: Experimental Setup for Optical Measurements). The time traces of the fluorescence signal were recorded from both the AuNIs-e-NA and a conventional nanoaperture.

Figure 3a and b show the time traces of fluorescence from the ICG solutions obtained with a conventional nanoaperture and the AuNIs-e-NA, respectively. Stronger intensity bursts were

observed in the fluorescence time trace obtained with the AuNIs-e-NA, where each burst corresponds to a single ICG fluorophore diffusing into the AuNIs-e-NA and interacting with the “hotspots” in the AuNIs. A wide range of magnitudes of the intensity bursts with a maximum of ~1500 counts/ms occur in the fluorescence signal measured using the AuNIs-e-NA, as shown in Figure 3c. The large variation in the magnitude of the intensity bursts arises from variations in the magnitude of the local-field intensities of multiple “hotspots” within the nanoaperture, the alignment of the fluorophore and the localized field, and the position of the fluorophore relative to the “hotspots”. A fluorophore that diffuses close to the vicinity of the highest-intensity “hotspot” with its dipole moment aligned with the localized electric field at the “hotspot” is expected to provide the maximum fluorescence intensity burst. In contrast to the strong intensity bursts consistently observed with the different AuNIs-e-NAs, the weak fluorescence bursts that were almost buried in the background signal were observed for single ICG molecules diffusing into a conventional nanoaperture (Figure 3a). The strong fluorescence intensity bursts for the AuNIs-e-NA prove the presence of multiple strong electromagnetic “hotspots” within the AuNIs-e-NA, in contrast to the weak and uniform field in the conventional nanoaperture.

To confirm that the fluorescence bursts were only from the ICG molecules instead of other entities in the solution, we performed control experiments in the absence of fluorophores, which showed no fluorescence intensity bursts. The magnitude of the intensity bursts was extracted from the time traces of the fluorescence signal and plotted as histograms (Figure 3c). We can see that the AuNIs-e-NA features a significant population of intensity bursts with the magnitude much larger than that obtained from the conventional nanoaperture. To further measure the fluorescence improvement by the AuNIs-e-NA over a conventional nanoaperture in the visible light regime, we performed similar experiments using two other fluorophores: crystal violet (CV) (excitation/emission wavelengths: 590/638 nm) and methylene blue (MB) (excitation/emission wavelengths: 656/677 nm) with quantum yields of 2% and 5%, respectively.[76,77] In our experiments, we used 532 and 660 nm laser beams to excite the CV and MB fluorophores, respectively. Similarly, we observed much stronger intensity bursts in the fluorescence signals collected from both fluorophores with the AuNIs-e-NA than those with the conventional nanoaperture (see Supporting Information, Figures S13 and S14).

Two major processes contributed to the fluorescence enhancement provided by the AuNIs-e-NA. One is that the AuNIs acted as nanoantennas that concentrated light to nanoscale volumes near their surfaces. The strong light concentration led to high absorption of light by the fluorophore molecules diffusing in the vicinity of the AuNIs, which is known as excitation enhancement (E_{exc}). The other is that the AuNI nanoantennas modified the radiative and nonradiative decay rates and thus the emission of the nearby fluorophore, which is termed emission enhancement (E_{ems}). Thus, the overall fluorescence enhancement is the product of excitation enhancement and emission enhancement ($E = E_{exc} \times E_{ems}$). It should be noted that the fluorescence can also be quenched when the fluorophore molecule comes too close to metal nanostructures.[78] The quenching can be associated with the coupling of fluorophore emission to the higher-order dark modes of the metal nanostructures. Figure 4 shows the fluorescence enhancement factors provided by the AuNIs-e-NA with reference to those provided by the conventional nanoaperture for CV,

MB, and ICG fluorophores excited with laser wavelengths of 532, 660, and 785 nm, respectively. It should be emphasized that the enhancement factors in Figure 4 account for the extra boost of the fluorescence signals that benefits from the introduction of AuNIs into the conventional nanoaperture and is beyond the signal enhancement by the conventional nanoaperture. A maximum fluorescence enhancement factor of greater than 100 was obtained for MB molecules, as shown in Figure 4b. The enhancement factors were smaller for CV molecules excited by a 532 nm laser beam, which were consistent with the smaller field enhancement provided by the AuNIs-e-NA at this wavelength (see Supporting Information, Figure S11). We believe that a better match of the excitation laser wavelengths with the gap plasmon resonance wavelengths by optimizing the compositions, shapes, and sizes of the nanoislands within the nanoaperture can further improve the fluorescence enhancement factors in single-molecule fluorescence spectroscopy for a wide range of molecular analytes.

We also calculated the individual fluorescence enhancements provided by a AuNIs-e-NA and a conventional nanoaperture through finite-difference time-domain (FDTD) simulations. The fluorescence enhancement factor of the AuNIs-e-NA with reference to the conventional nanoaperture is given by[79]

$$\text{Enhancement factor} = \frac{E_{\text{AuNIs-e-NA}}}{E_{\text{NA}}} \tag{1}$$

where

$$E_{\text{NA, AuNIs-e-NA}} = E_{\text{exc}} \times E_{\text{ems}} \tag{2}$$

$$E_{\text{exc}} = \frac{|E|^2}{|E_{\text{o}}|^2} \tag{3}$$

$$E_{\text{ems}} = \frac{\Gamma_{\text{rad}}}{\Gamma^{\text{o}}_{\text{rad}}} \frac{1}{1 - \varphi_{\text{o}} + \varphi_{\text{o}}\left(\frac{\Gamma_{\text{rad}}}{\Gamma^{\text{o}}_{\text{rad}}} + \frac{\Gamma_{\text{loss}}}{\Gamma^{\text{o}}_{\text{rad}}}\right)} \tag{4}$$

where $E_{\text{AuNIs-e-NA}}$ and E_{NA} are the overall fluorescence enhancement factors from AuNIs-e-NA and a conventional nanoaperture, respectively. $|E|^2$ and $|E_{\text{o}}|^2$ are the magnitudes of the electric-field intensity with and without the nanoaperture. Γ_{rad} and $\Gamma_{\text{o}}^{\text{rad}}$ are the radiative decay rates in the system with and without the nanoaperture. Γ_{loss} is the nonradiative decay rate transitions in the emitter with the nanoaperture, and φ_{o} is the intrinsic quantum yield of the fluorescent dye. The excitation enhancement values (like those in Figure 2d), along with the simulated normalized radiative $\frac{\Gamma_{\text{rad}}}{\Gamma^{\text{o}}_{\text{rad}}}$ and nonradiative $\frac{\Gamma_{\text{los}}}{\Gamma^{\text{o}}_{\text{rad}}}$ decay rates, were used to calculate the overall fluorescence enhancement factor for the AuNIs-e-NA and the conventional nanoaperture and the enhancement factor (see Supplementary Note 4).

The enhancement factors obtained experimentally (Figure 4) were found to be within an order of magnitude of those estimated through simulations (see Supporting Information, Figure S15). The small deviation of the simulated values from the experimental ones arises due to the averaging of the normalized radiative and nonradiative decay rates in the simulations, which otherwise showed a 30–50% variation in the magnitudes depending on the position of the dipole emitter within the AuNIs-e-NA. Also, the variation in the AuNIs distribution and the approximate modeling of the nanoislands as nanocylinders impacted the simulated field and excitation enhancement values. More specifically, the experimentally measured fluorescence enhancement factors for AuNIs-e-NA excited by different wavelengths showed a wide range of values, which is consistent with the presence of multiple high-intensity regions of different magnitudes resulting in the large variance in the excitation enhancement seen by the fluorophores. AuNIs-e-NA excited by 660 and 785 nm wavelength lasers showed fluorescence burst events with the higher enhancement factors compared to those excited by a 532 nm laser beam. This is due to the large difference between the magnitude of the field enhancements provided by AuNIs-e-NA, when excited by 532 nm compared to 660 and 785 nm laser beams. On the basis of our theoretically estimated enhancement factors (electric field enhancement + emission enhancement) for 660 and 785 nm laser excitation (see Supporting Information, Figure S15), we expect to observe events with the higher fluorescence enhancement factors when the AuNIs-e-NA is excited by a 785 nm laser beam compared to 660 nm. However, these highest-enhancement events can only occur when the fluorophore molecule accesses the high field intensity regions excited by the 785 nm laser beam. Since there exist only a few pixels (<7, pixel size: 9 nm^2) with the highest field intensities within the AuNIs-e-NA, the events with high fluorescence enhancement factors are rare, making it difficult to observe such events within our experimental time (i.e., 10 s). In addition, the difference in the quantum yield of the MB and ICG fluorophores can also influence the fluorescence enhancement factors, where the higher quantum-yield fluorophores showed a smaller fluorescence enhancement factor as reported earlier.[80] By collecting the fluorescence data over a longer period of time for the different AuNIs-e-NAs, one could capture the rare events with the high fluorescence enhancement when excited by a laser beam with a wavelength of 785 nm.

In summary, the AuNIs-e-NA combines the advantages of both “nanoantenna” and “nanoaperture” in a simple and robust hybrid structure. With its small detection volume and background-free operation, in combination with multiple “hotspots” with strong field intensities, the AuNIs-e-NA significantly enhances the fluorescence signal of single molecules. The simple design, easy fabrication, and ability to operate over a wide range of laser wavelengths and arbitrary laser polarizations make the AuNIs-e-NA a more attractive choice over other modified-nanoaperture designs.[60,62] However, the fabrication process lacks precise control of the morphology, size, and gap of the nanoantennas in the AuNIs-e-NA, which can cause variation in the optical response of the substrates and thus the fluorescence signals, limiting their uses in highly precise measurements. The concept of nanoislands in a nanoaperture is applicable to various nanoapertures with arbitrary shapes, sizes, and materials, where the properties of both nanoapertures and nanoislands can be optimized to achieve the best spectroscopic performance at any desired wavelength. We envision that, due to its simplicity and robustness, such a hybrid nanoaperture design

can be readily applied to improve performances of various optical spectroscopies and devices where conventional nanoapertures have traditionally been used such as optical sensing, optical trapping, Raman spectroscopy, and fluorescence correlation spectroscopy.[81] In addition, we foresee that the AuNIs-e-NA will become a promising platform that effectively harnesses optothermal effects for applications in optothermal nanoreactors[82] and optothermal tweezers.[83,84]

METHODS

Sample Fabrication.

Colloidal lithography was used to fabricate the AuNIs-e-NAs. First, thin Au films with a thickness of 4.5 nm were deposited (Denton thermal evaporator, base pressure: 9×10^{-6} Torr, deposition rate: 0.1 Å/s) on glass coverslips (Thermofischer Scientific, No. 1) followed by thermal annealing using a box furnace (Thermo Scientific Lindberg/Blue M box furnace) at 550 °C in air for 2 h to form AuNIs. Subsequently, monodisperse polystyrene spheres with a diameter of 200 nm were spin-coated on the AuNIs to form randomly distributed arrays, which served as masks to form the nanoapertures through sequential thermal deposition of 10 nm chromium and 100 nm Au or Ag films (Denton thermal evaporator, base pressure: 9×10^{-6} Torr, deposition rate: 0.5 Å/s). Polystyrene spheres were then removed using Scotch tape, which resulted in the formation of a large number of AuNIs-e-NAs on the glass coverslips. The substrates were later soaked in toluene for 2–3 h to remove the residual polystyrene and finally rinsed with acetone, isopropyl alcohol, and deionized water before use. The size and shape of the AuNIs-e-NAs can be controlled by using specific colloidal particles as masks. For example, AuNIs-e-NAs of some basic geometries such as rectangular, triangular, or double-nanohole can be fabricated by using nanorods, nanoprisms, or dimers as masks in the fabrication process.

Chemicals for Fluorescence and Raman Spectroscopies.

We performed the fluorescence measurements with crystal violet (Thermo Fisher Scientific), methylene blue, and indocyanine green (VWR International) dispersed in 1:1 water–glycerol solvent at a concentration of 100 nM, respectively. A 50% glycerol solution was prepared by diluting the as-purchased glycerol (Fisher Scientific) with deionized water.

Experimental Setup for Optical Measurements.

The optical measurements were performed using an inverted microscope (Nikon Eclipse Ti-E). For the fluorescence signal measurement, a circularly polarized laser beam was focused using a 100× oil immersion objective lens (Nikon, NA = 1.25) on a single nanoaperture using a three-axis stage. Three different laser beams with wavelengths of 532 (Coherent, Genesis MX STM-1W), 660 (Laser Quantum, Ventus), and 785 nm (Thorlabs, L785P090) were used to excite the crystal violet, methylene blue and indocyanine green fluorophore molecules, respectively. The fluorescence signal was collected in the back-reflection mode using the same objective lens and detected using a fast sCMOS camera (Andor, Zyla 4.2) with an acquisition time of 1 ms. Although an avalanche photodiode with a higher detection sensitivity and temporal resolution would be a better choice for carrying out the fluorescence measurement from a single nanoaperture, our fast sCMOS camera provides enough

sensitivity to detect the strong fluorescence signal from the AuNI-e-NA and sufficient temporal resolution (1 ms) to capture the dynamics of slowly diffusing fluorophores in a water–glycerol-filled nanoaperture. The fluorescence signal from an individual nanoaperture was collected by drawing a custom region-of-interest (ROI) around the nanoaperture image (see Supporting Information, Figure S16). The image size was cropped to 20 × 20 pixels during the signal capture for the faster acquisition, and the fluorescence signal was obtained by integrating the intensity within the ROI consisting of 82 pixels over an integration time of 1 ms. For transmission spectrum measurements, the signal was directed to an Andor spectrometer coupled with a liquid-nitrogen-cooled CCD camera. The spectrometer was set to 600 grooves per mm grating and a 100 μm entrance slit.

Numerical Simulations.

The FDTD method (Lumerical 2020a) was used for three-dimensional electromagnetic modeling of the AuNIs-e-NA and the conventional nano-aperture. The nanoaperture model consisted of a circular hole with a diameter of 200 nm made on a silver film with a thickness of 100 nm on a glass substrate. The inside and surrounding of the nanoaperture were filled with water (refractive index = 1.33). To model the AuNIs-e-NA, a SEM image of the AuNIs was imported into the model (see Supplementary Note 5). The image was scaled appropriately for an accurate modeling of nanoparticles sizes and spacing and was assigned with material properties of Au. The AuNIs were placed at the bottom interface of the glass substrate and water within the nanoaperture. It should be noted that, while the shapes, sizes, and spatial distributions of the Au nanoparticles constituting the AuNIs were modeled precisely from the SEM image, the lack of cross-sectional information resulted in approximating the nanoparticles as nanocylinders with a constant height of 20 nm. The optical constants of Au and Ag were taken from Johnson and Christy,[85] and the refractive index of the glass substrate was set as 1.52. Perfectly matched layers were utilized as the boundary conditions for all directions. A Gaussian laser beam was used as the excitation source and launched from the glass substrate side. The electromagnetic intensity was measured using a monitor located at a plane a few nanometers above the AuNIs in the nanoaperture.

Supplementary Material

Refer to Web version on PubMed Central for supplementary material.

ACKNOWLEDGMENTS

The authors would like to acknowledge the financial support from the National Science Foundation (NSF-ECCS-2001650), the National Aeronautics and Space Administration (80NSSC17K0520), and the National Institute of General Medical Sciences of the National Institutes of Health (DP2GM128446). They also thank the Texas Advanced Computing Center (TACC) at The University of Texas at Austin for providing high-performance computing resources.

REFERENCES

(1). Flauraud V; van Zanten TS; Mivelle M; Manzo C; Garcia Parajo MF; Brugger J Large-Scale Arrays of Bowtie Nanoaperture Antennas for Nanoscale Dynamics in Living Cell Membranes. Nano Lett. 2015, 15, 4176–4182. [PubMed: 25926327]

(2). Olson SAO; Mohr DA; Shaver J; Johnson TW; Oh S-H Plasmonic Cup Resonators for Single-Nanohole-Based Sensing and Spectroscopy. ACS Photonics 2016, 3, 1202–1207.

(3). Wang Y; Zijlstra P Plasmon-Enhanced Single-Molecule Enzymology. ACS Photonics 2018, 5, 3073–3081. [PubMed: 30148184]

(4). Prasad A; Choi J; Jia Z; Park S; Gartia MR Nanohole Array Plasmonic Biosensors: Emerging Point-of-Care Applications. Biosens. Bioelectron 2019, 130, 185–203. [PubMed: 30738247]

(5). Kotnala A; DePaoli D; Gordon R Sensing Nanoparticles Using a Double Nanohole Optical Trap. Lab Chip 2013, 13, 4142–4146. [PubMed: 23969596]

(6). Ghenuche P; de Torres J; Moparthi SB; Grigoriev V; Wenger J Nanophotonic Enhancement of the Förster Resonance Energy-Transfer Rate with Single Nanoapertures. Nano Lett. 2014, 14, 4707–4714. [PubMed: 25020141]

(7). Zhang W; Fang Z; Zhu X Near-Field Raman Spectroscopy with Aperture Tips. Chem. Rev 2017, 117, 5095–5109. [PubMed: 27977167]

(8). Jahr N; Anwar M; Stranik O; Hädrich N; Vogler N; Csaki A; Popp J; Fritzsche W Spectroscopy on Single Metallic Nanoparticles Using Subwavelength Apertures. J. Phys. Chem. C 2013, 117, 7751–7756.

(9). Fore S; Yuen Y; Hesselink L; Huser T Pulsed-Interleaved Excitation FRET Measurements on Single Duplex DNA Molecules Inside C-Shaped Nanoapertures. Nano Lett. 2007, 7, 1749–1756. [PubMed: 17503872]

(10). Xie Z; Lefier Y; Suarez MA; Mivelle M; Salut R; Merolla J-M; Grosjean T Doubly Resonant Photonic Antenna for Single Infrared Quantum Dot Imaging at Telecommunication Wavelengths. Nano Lett. 2017, 17, 2152–2158. [PubMed: 28339208]

(11). Mivelle M; van Zanten TS; Garcia-Parajo MF Hybrid Photonic Antennas for Subnanometer Multicolor Localization and Nanoimaging of Single Molecules. Nano Lett. 2014, 14, 4895–4900. [PubMed: 25050445]

(12). Wang L; Uppuluri SM; Jin EX; Xu X Nanolithography Using High Transmission Nanoscale Bowtie Apertures. Nano Lett. 2006, 6, 361–364. [PubMed: 16522023]

(13). Hu H; Yeom J; Mensing G; Chen Y; Shannon MA; King WP Nano-Fabrication with a Flexible Array of Nano-Apertures. Nanotechnology 2012, 23, 175303. [PubMed: 22481526]

(14). Koya AN; Cunha J; Guo T-L; Toma A; Garoli D; Wang T; Juodkazis S; Cojoc D; Proietti Zaccaria R Novel Plasmonic Nanocavities for Optical Trapping-Assisted Biosensing Applications. Adv. Opt. Mater 2020, 8, 1901481.

(15). Juan ML; Gordon R; Pang Y; Eftekhari F; Quidant R Self-Induced Back-Action Optical Trapping of Dielectric Nanoparticles. Nat. Phys 2009, 5, 915–919.

(16). Kotnala A; Gordon R Quantification of High-Efficiency Trapping of Nanoparticles in a Double Nanohole Optical Tweezer. Nano Lett. 2014, 14, 853–856. [PubMed: 24404888]

(17). Schön P; Bonod N; Devaux E; Wenger J; Rigneault H; Ebbesen TW; Brasselet S Enhanced Second-Harmonic Generation from Individual Metallic Nanoapertures. Opt. Lett 2010, 35, 4063–4065. [PubMed: 21124613]

(18). Fujimoto K; Morita Y; Iino R; Tomishige M; Shintaku H; Kotera H; Yokokawa R Simultaneous Observation of Kinesin-Driven Microtubule Motility and Binding of Adenosine Triphosphate Using Linear Zero-Mode Waveguides. ACS Nano 2018, 12, 11975–11985. [PubMed: 30418736]

(19). Zhu P; Craighead HG Zero-Mode Waveguides for Single-Molecule Analysis. Annu. Rev. Biophys 2012, 41, 269–293. [PubMed: 22577821]

(20). Levene MJ; Korlach J; Turner SW; Foquet M; Craighead HG; Webb WW Zero-Mode Waveguides for Single-Molecule Analysis at High Concentrations. Science (Washington, DC, U. S.) 2003, 299, 682–686.

(21). Rigneault H; Capoulade J; Dintinger J; Wenger J; Bonod N; Popov E; Ebbesen TW; Lenne P-F Enhancement of Single-Molecule Fluorescence Detection in Subwavelength Apertures. Phys. Rev. Lett 2005, 95, 117401. [PubMed: 16197045]

(22). Samiee KT; Foquet M; Guo L; Cox EC; Craighead HG λ -Repressor Oligomerization Kinetics at High Concentrations Using Fluorescence Correlation Spectroscopy in Zero-Mode Waveguides. Biophys. J 2005, 88, 2145–2153. [PubMed: 15613638]

(23). Jensen RA; Huang I; Chen O; Choy JT; Bischof TS; Lončar M; Bawendi MG Optical Trapping and Two-Photon Excitation of Colloidal Quantum Dots Using Bowtie Apertures. ACS Photonics 2016, 3, 423–427.

(24). Liu GL; Kim J; Lu Y; Lee LP Fluorescence Enhancement of Quantum Dots Enclosed in Au Nanopockets with Subwavelength Aperture. Appl. Phys. Lett 2006, 89, 241118.

(25). Hacohen N; Ip CJX; Gordon R Analysis of Egg White Protein Composition with Double Nanohole Optical Tweezers. ACS Omega 2018, 3, 5266–5272. [PubMed: 31458737]

(26). Al Balushi AA; Kotnala A; Wheaton S; Gelfand RM; Rajashekara Y; Gordon R Label-Free Free-Solution Nanoaperture Optical Tweezers for Single Molecule Protein Studies. Analyst 2015, 140, 4760–4778. [PubMed: 25734189]

(27). Kotnala A; Wheaton S; Gordon R Playing the Notes of DNA with Light: Extremely High Frequency Nanomechanical Oscillations. Nanoscale 2015, 7, 2295–2300. [PubMed: 25584811]

(28). Kotnala A; Gordon R Double Nanohole Optical Tweezers Visualize Protein P53 Suppressing Unzipping of Single DNA-Hairpins. Biomed. Opt. Express 2014, 5, 1886–1894. [PubMed: 24940547]

(29). Larkin J; Henley RY; Jadhav V; Korlach J; Wanunu M Length-Independent DNA Packing into Nanopore Zero-Mode Waveguides for Low-Input DNA Sequencing. Nat. Nanotechnol 2017, 12, 1169–1175. [PubMed: 28892102]

(30). Jin EX; Xu X Focussed Ion Beam Machined Cantilever Aperture Probes for Near-Field Optical Imaging. J. Microsc 2008, 229, 503–511. [PubMed: 18331502]

(31). Punj D; de Torres J; Rigneault H; Wenger J Gold Nanoparticles for Enhanced Single Molecule Fluorescence Analysis at Micromolar Concentration. Opt. Express 2013, 21, 27338–27343. [PubMed: 24216956]

(32). Popov E; Nèviere M; Wenger J; Lenne P; Rigneault H; Chaumet P; Dintinger J; Ebbesen T Field Enhancement in Single Subwavelength Apertures. J. Opt. Soc. Am. A2006, 23, 2342–2348.

(33). Jiang Q; Rogez B; Claude J-B; Baffou G; Wenger J Temperature Measurement in Plasmonic Nanoapertures Used for Optical Trapping. ACS Photonics 2019, 6, 1763–1773.

(34). Wu LY; Ross BM; Lee LP Optical Properties of the Crescent-Shaped Nanohole Antenna. Nano Lett. 2009, 9, 1956–1961. [PubMed: 19354226]

(35). Alaverdyan Y; Sepúlveda B; Eurenius L; Olsson E; Käll M Optical Antennas Based on Coupled Nanoholes in Thin Metal Films. Nat. Phys 2007, 3, 884–889.

(36). Lu G; Li W; Zhang T; Yue S; Liu J; Hou L; Li Z; Gong Q Plasmonic-Enhanced Molecular Fluorescence within Isolated Bowtie Nano-Apertures. ACS Nano 2012, 6, 1438–1448. [PubMed: 22247937]

(37). Wu M; Liu W; Hu J; Zhensheng Zhong TR; Zhou L; Cai X; Ma J Fluorescence Enhancement in an Over-Etched Gold Zero-Mode Waveguide. Opt. Express 2019, 27, 19002–19018. [PubMed: 31252834]

(38). Ponzellini P; Zambrana-Puyalto X; Maccaferri N; Lanzanò L; De Angelis F; Garoli D Plasmonic Zero Mode Waveguide for Highly Confined and Enhanced Fluorescence Emission. Nanoscale 2018, 10, 17362–17369. [PubMed: 30199084]

(39). Mahdavi F; Blair S Nanoaperture Fluorescence Enhancement in the Ultraviolet. Plasmonics 2010, 5, 169–174.

(40). Djaker N; Hostein R; Devaux E; Ebbesen TW; Rigneault H; Wenger J Surface Enhanced Raman Scattering on a Single Nanometric Aperture. J. Phys. Chem. C 2010, 114, 16250–16256.

(41). Wenger J; Cluzel B; Dintinger J; Bonod N; Fehrembach A-L; Popov E; Lenne P-F; Ebbesen TW; Rigneault H Radiative and Nonradiative Photokinetics Alteration Inside a Single Metallic Nanometric Aperture. J. Phys. Chem. C 2007, 111, 11469–11474.

(42). Wenger J; Gérard D; Rigneault H; Lowder B; Blair S; Devaux E; Ebbesen TW Nanoaperture-Enhanced Signal-to-Noise Ratio in Fluorescence Correlation Spectroscopy. Anal. Chem 2009, 81, 834–839. [PubMed: 19099408]

(43). Mivelle M; van Zanten TS; Neumann L; van Hulst NF; Garcia-Parajo MF Ultrabright Bowtie Nanoaperture Antenna Probes Studied by Single Molecule Fluorescence. Nano Lett. 2012, 12, 5972–5978. [PubMed: 23098104]

(44). Aouani H; Mahboub O; Devaux E; Rigneault H; Ebbesen TW; Wenger J Plasmonic Antennas for Directional Sorting of Fluorescence Emission. Nano Lett. 2011, 11, 2400–2406. [PubMed: 21591739]

(45). Dutta Choudhury S; Ray K; Lakowicz JR Silver Nanostructures for Fluorescence Correlation Spectroscopy: Reduced Volumes and Increased Signal Intensities. J. Phys. Chem. Lett 2012, 3, 2915–2919. [PubMed: 26855696]

(46). Cambiasso J; König M; Cortés E; Schlücker S; Maier SA Surface-Enhanced Spectroscopies of a Molecular Monolayer in an All-Dielectric Nanoantenna. ACS Photonics 2018, 5, 1546–1557.

(47). Muskens OL; Giannini V; Sánchez-Gil JA; Gómez Rivas J Strong Enhancement of the Radiative Decay Rate of Emitters by Single Plasmonic Nanoantennas. Nano Lett. 2007, 7, 2871–2875. [PubMed: 17683156]

(48). Darvill D; Centeno A; Xie F Plasmonic Fluorescence Enhancement by Metal Nanostructures: Shaping the Future of Bionanotechnology. Phys. Chem. Chem. Phys 2013, 15, 15709–15726. [PubMed: 23579473]

(49). Vietz C; Kaminska I; Sanz Paz M; Tinnefeld P; Acuna GP Broadband Fluorescence Enhancement with Self-Assembled Silver Nanoparticle Optical Antennas. ACS Nano 2017, 11, 4969–4975. [PubMed: 28445644]

(50). Mertens H; Koenderink AF; Polman A Plasmon-Enhanced Luminescence near Noble-Metal Nanospheres: Comparison of Exact Theory and an Improved Gersten and Nitzan Model. Phys. Rev. B: Condens. Matter Mater. Phys 2007, 76, 115123.

(51). Kühn S; Håkanson U; Rogobete L; Sandoghdar V Enhancement of Single-Molecule Fluorescence Using a Gold Nanoparticle as an Optical Nanoantenna. Phys. Rev. Lett 2006, 97, 17402.

(52). Khatua S; Paulo PMR; Yuan H; Gupta A; Zijlstra P; Orrit M Resonant Plasmonic Enhancement of Single-Molecule Fluorescence by Individual Gold Nanorods. ACS Nano 2014, 8, 4440–4449. [PubMed: 24684549]

(53). Lu X; Ye G; Punj D; Chiechi RC; Orrit M Quantum Yield Limits for the Detection of Single-Molecule Fluorescence Enhancement by a Gold Nanorod. ACS Photonics 2020, 7, 2498–2505.

(54). Punj D; Regmi R; Devilez A; Plauchu R; Moparthi SB; Stout B; Bonod N; Rigneault H; Wenger J Self-Assembled Nanoparticle Dimer Antennas for Plasmonic-Enhanced Single-Molecule Fluorescence Detection at Micromolar Concentrations. ACS Photonics 2015, 2, 1099–1107.

(55). Sugimoto H; Yashima S; Fujii M Hybridized Plasmonic Gap Mode of Gold Nanorod on Mirror Nanoantenna for Spectrally Tailored Fluorescence Enhancement. ACS Photonics 2018, 5, 3421–3427.

(56). Puchkova A; Vietz C; Pibiri E; Wünsch B; Sanz Paz M; Acuna GP; Tinnefeld P DNA Origami Nanoantennas with over 5000-Fold Fluorescence Enhancement and Single-Molecule Detection at 25 MM. Nano Lett. 2015, 15, 8354–8359. [PubMed: 26523768]

(57). Kinkhabwala A; Yu Z; Fan S; Avlasevich Y; Müllen K; Moerner WE Large Single-Molecule Fluorescence Enhancements Produced by a Bowtie Nanoantenna. Nat. Photonics 2009, 3, 654–657.

(58). Cheng X; Lotubai E; Rodriguez M; Wang Y UV Fluorescence Enhancement by Aluminum and Magnesium Equilateral Bowtie Nanoantennas. OSA Contin. 2020, 3, 3300–3313.

(59). Curto AG; Volpe G; Taminiau TH; Kreuzer MP; Quidant R; van Hulst NF Unidirectional Emission of a Quantum Dot Coupled to a Nanoantenna. Science (Washington, DC, U. S.) 2010, 329, 930LP–933.

(60). Aouani H; Mahboub O; Devaux E; Rigneault H; Ebbesen TW; Wenger J Large Molecular Fluorescence Enhancement by a Nanoaperture with Plasmonic Corrugations. Opt. Express 2011, 19, 13056–13062. [PubMed: 21747457]

(61). Melentiev PN; Afanasiev AE; Kuzin AA; Zablotskiy AV; Baturin AS; Balykin VI Extremely High Transmission of Light through a Nanohole inside a Photonic Crystal. J. Exp. Theor. Phys 2012, 115, 185–193.

(62). Punj D; Mivelle M; Moparthi SB; van Zanten TS; Rigneault H; van Hulst NF; García-Parajó MF; Wenger J A Plasmonic 'Antenna-in-Box' Platform for Enhanced Single-Molecule Analysis at Micromolar Concentrations. Nat. Nanotechnol 2013, 8, 512–516. [PubMed: 23748196]

(63). Kang M; Park S-G; Jeong K-H Repeated Solid-State Dewetting of Thin Gold Films for Nanogap-Rich Plasmonic Nanoislands. Sci. Rep 2015, 5, 14790. [PubMed: 26469768]

(64). Milewska A; Zivanovic V; Merk V; Arnalds UB; Sigurjónsson ÓE; Kneipp J; Leosson K Gold Nanoisland Substrates for SERS Characterization of Cultured Cells. Biomed. Opt. Express 2019, 10, 6172–6188. [PubMed: 31853393]

(65). Portela A; Calvo-Lozano O; Estevez M-C; Medina Escuela A; Lechuga LM Optical Nanogap Antennas as Plasmonic Biosensors for the Detection of MiRNA Biomarkers. J. Mater.Chem. B 2020, 8, 4310–4317. [PubMed: 32329505]

(66). Syrenova S; Wadell C; Langhammer C Shrinking-Hole Colloidal Lithography: Self-Aligned Nanofabrication of Complex Plasmonic Nanoantennas. Nano Lett. 2014, 14, 2655–2663. [PubMed: 24697350]

(67). Gu P; Zhang W; Zhao Z; Ai B; Zheng T; Chiechi RC; Li C; Shi Z; Zhang G Engineering Colloidal Lithography and Nanoskiving to Fabricate Rows of Opposing Crescent Nanogaps. Adv. Opt. Mater 2020, 8, 2000006.

(68). Ravindranath AL; Shariatdoust MS; Mathew S; Gordon R Colloidal Lithography Double-Nanohole Optical Trapping of Nanoparticles and Proteins. Opt. Express 2019, 27, 16184–16194. [PubMed: 31163802]

(69). Cesaria M; Taurino A; Manera MG; Minunni M; Scarano S; Rella R Gold Nanoholes Fabricated by Colloidal Lithography: Novel Insights into Nanofabrication, Short-Range Correlation and Optical Properties. Nanoscale 2019, 11, 8416–8432. [PubMed: 30985849]

(70). Jamiolkowski RM; Chen KY; Fiorenza SA; Tate AM; Pfeil SH; Goldman YE Nanoaperture Fabrication via Colloidal Lithography for Single Molecule Fluorescence Analysis. PLoS One 2019, 14, No. e0222964. [PubMed: 31600217]

(71). Ravindranath AL; Mirali Seyed S; Mathew S; Gordon R Colloidal Lithography Double-Nanohole Optical Trapping of Nanoparticles and Proteins. Opt. Express 2019, 27, 16184–16194. [PubMed: 31163802]

(72). Gupta G; Tanaka D; Ito Y; Shibata D; Shimojo M; Furuya K; Mitsui K; Kajikawa K Absorption Spectroscopy of Gold Nanoisland Films: Optical and Structural Characterization. Nanotechnology 2009, 20, 25703.

(73). Bonyár A; Csarnovics I; Veres M; Himics L; Csik A; Kámán J; Balázs L; Kökényesi S Investigation of the Performance of Thermally Generated Gold Nanoislands for LSPR and SERS Applications. Sens. Actuators, B 2018, 255, 433–439.

(74). Serrano A; Rodríguez de la Fuente O; García MA Extended and Localized Surface Plasmons in Annealed Au Films on Glass Substrates. J. Appl. Phys 2010, 108, 74303.

(75). Zhang D; Qiu D; Chen Y; Wang R; Zhu L; Wang P; Ming H; Badugu R; Stella U; Descrovi E; et al. Coupling of Fluorophores in Single Nanoapertures with Tamm Plasmon Structures. J. Phys. Chem. C 2019, 123, 1413–1420.

(76). Taniguchi M; Lindsey JS Database of Absorption and Fluorescence Spectra of > 300 Common Compounds for Use in PhotochemCAD. Photochem. Photobiol 2018, 94, 290–327. [PubMed: 29166537]

(77). Taniguchi M; Du H; Lindsey JS PhotochemCAD 3: Diverse Modules for Photophysical Calculations with Multiple Spectral Databases. Photochem. Photobiol 2018, 94, 277–289. [PubMed: 29166541]

(78). Anger P; Bharadwaj P; Novotny L Enhancement and Quenching of Single-Molecule Fluorescence. Phys. Rev. Lett 2006, 96, 113002. [PubMed: 16605818]

(79). Aouani H; Mahboub O; Bonod N; Devaux E; Popov E; Rigneault H; Ebbesen TW; Wenger J Bright Unidirectional Fluorescence Emission of Molecules in a Nanoaperture with Plasmonic Corrugations. Nano Lett. 2011, 11, 637–644. [PubMed: 21247202]

(80). Regmi R; Al Balushi AA; Rigneault H; Gordon R; Wenger J Nanoscale Volume Confinement and Fluorescence Enhancement with Double Nanohole Aperture. Sci. Rep 2015, 5, 15852. [PubMed: 26511149]

(81). Kotnala A; Kollipara PS; Li J; Zheng Y Overcoming Diffusion-Limited Trapping in Nanoaperture Tweezers Using OptoThermal-Induced Flow. Nano Lett. 2020, 20, 768–779. [PubMed: 31834809]

(82). Saksena BD The Complete Raman Spectrum of Glycerine. Proc. - Indian Acad. Sci., Sect. A 1939, 10, 333.

(83). Lin L; Wang M; Peng X; Lissek EN; Mao Z; Scarabelli L; Adkins E; Coskun S; Unalan HE; Korgel BA; et al. Opto-Thermoelectric Nanotweezers. Nat. Photonics 2018, 12, 195–201. [PubMed: 29785202]

(84). Kotnala A; Zheng Y Opto-Thermophoretic Fiber Tweezers. Nanophotonics 2019, 8, 475–485. [PubMed: 34290953]

(85). Johnson PB; Christy RW Optical Constants of the Noble Metals. Phys. Rev. B 1972, 6, 4370–4379.

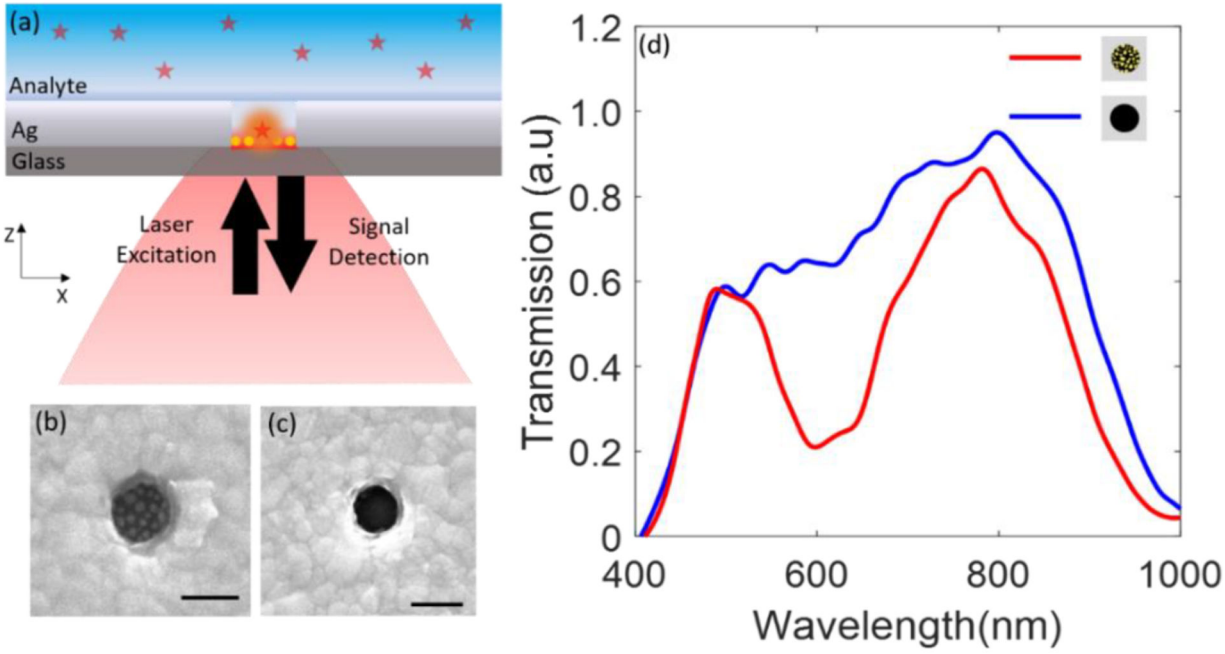

Figure 1.

(a) Schematic illustration (cross-sectional view) of the proposed hybrid AuNIs-e-NA structure and experimental setup for enhanced optical spectroscopies. (b, c) Scanning electron microscope (SEM) images (planar view) of a AuNIs-e-NA and a conventional nanoaperture, respectively. Scale bars: 200 nm. (d) Normalized optical transmission spectra experimentally measured from a conventional nanoaperture (blue curve) and a AuNIs-e-NA (red curve), as indicated by the inset schematics.

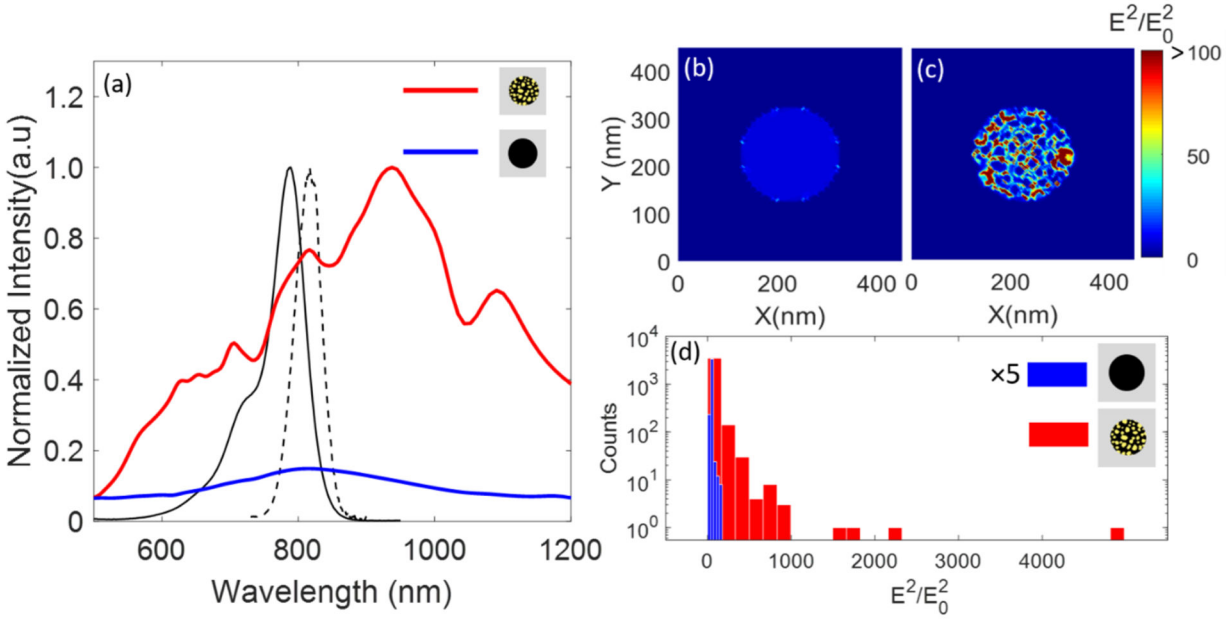

Figure 2.

Total electric-field intensities within a AuNIs-e-NA (red) and a conventional nanoaperture (blue) as a function of the excitation light wavelength. The field intensity values were normalized with respect to the maximum intensity within the given wavelength range. The two narrower curves (black) are the optical absorption (solid) and emission (dashed) spectra of the ICG fluorophore. (b, c) Simulated normalized electric-field intensity (or field enhancement) distributions within a conventional nanoaperture and a AuNIs-e-NA, respectively, when excited by a circularly polarized light with a wavelength of 785 nm. (d) Histograms comparing the intensities occurring within the AuNIs-e-NA (red) and conventional nanoaperture (blue) shown in (b) and (c). The monitor for recording the field intensity in the *xy* plane was placed 1 nm above the AuNIs. The insets in (a) and (d) are pictorial representations of the AuNIs-e-NA and conventional nanoaperture.

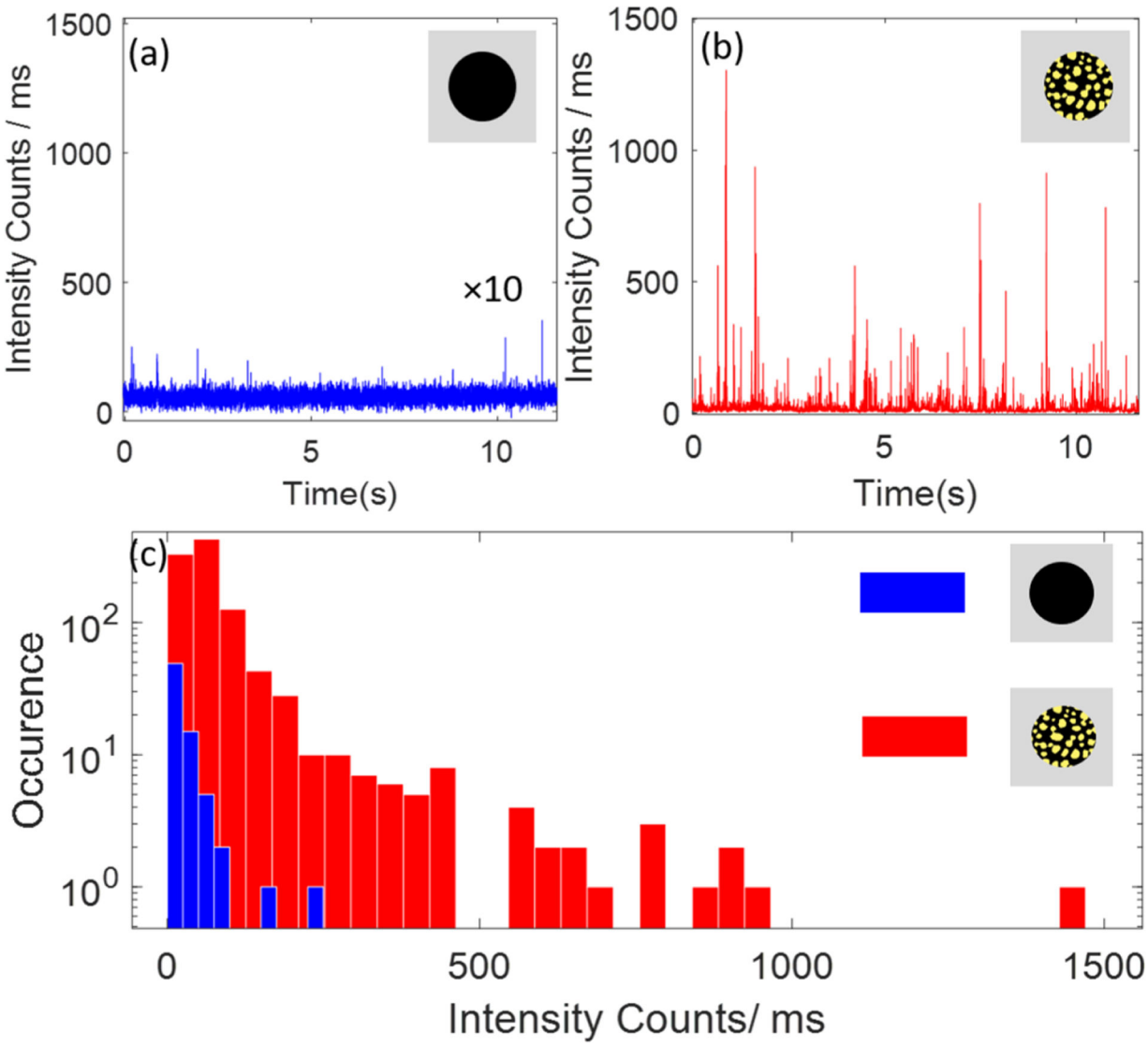

Figure 3.

Time traces of fluorescence signals measured from ICG fluorophores diffusing in (a) a conventional nanoaperture and (b) a AuNIs-e-NA. The substrates were covered with 100 nM ICG in 1:1 water–glycerol, which allowed the single-molecule fluorescence measurements. (c) Histograms comparing the magnitudes of the intensity bursts extracted from the fluorescence time traces for the conventional nanoaperture and the AuNIs-e-NA.

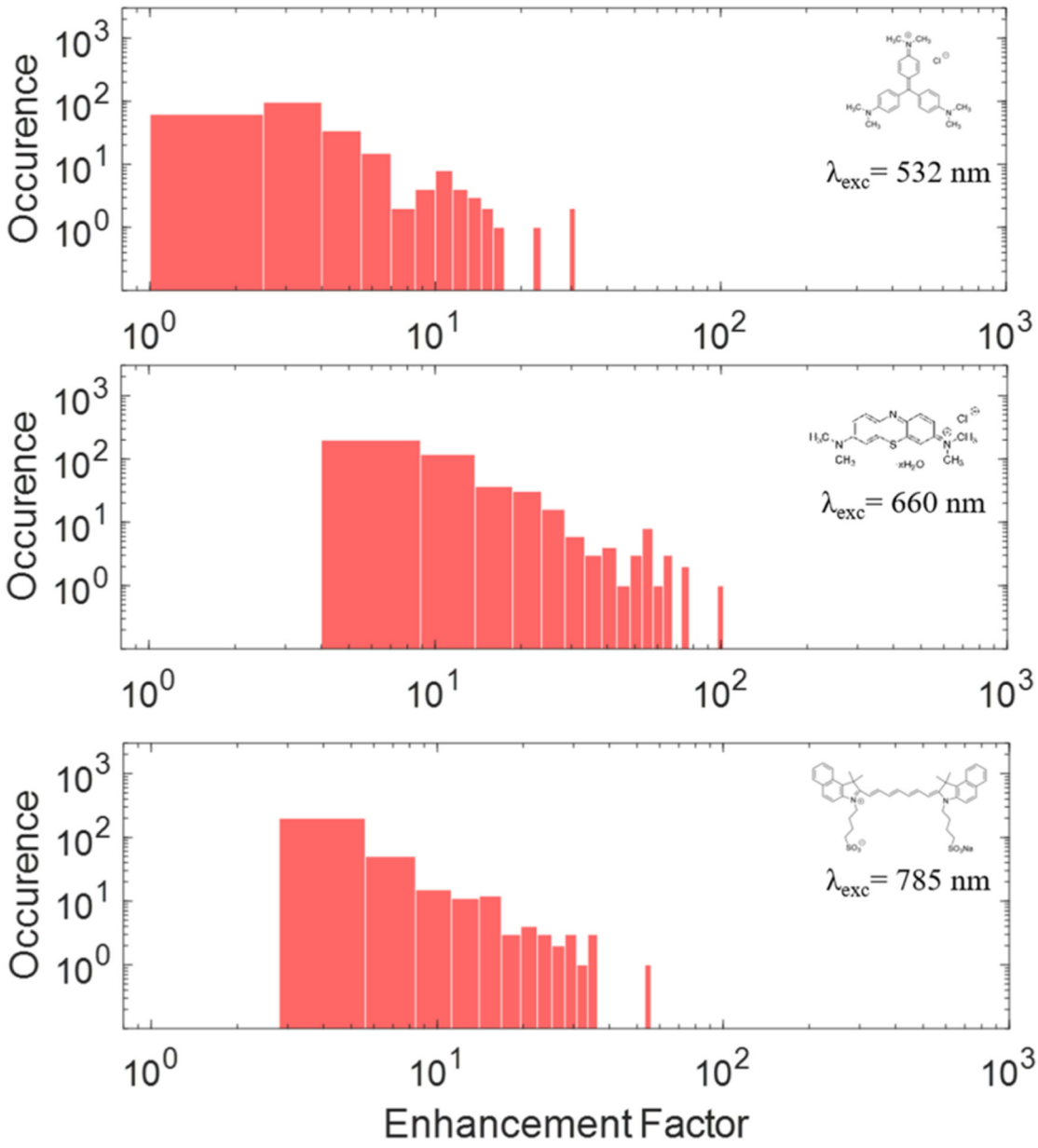

Figure 4.

Histograms showing the range of experimentally measured fluorescence enhancement factors for the AuNIs-e-NA with reference to those for the conventional nanoaperture for three different fluorophore molecules: (a) crystal violet, (b) methylene blue, and (c) indocyanine green excited at wavelengths (λ_{exc}) of 532, 660, and 785 nm, respectively. The insets show the molecular structures of the corresponding fluorophores.